Journal of Materials Chemistry A

PAPER

View Article Online
View Journal | View Issue

Cite this: J. Mater. Chem. A, 2019, 7, 14042

Monolayer GaS with high ion mobility and capacity as a promising anode battery material†

Xiuying Zhang,[a] Chen Yang,[ab] Yuanyuan Pan,[a] Mouyi Weng,[c] Linqiang Xu,[a] Shiqi Liu,[a] Jie Yang,[a] Jiahuan Yan,[a] Jingzhen Li,[a] Bowen Shi,[a] Jinbo Yang,[ade] Jiaxin Zheng,*[c] Feng Pan*[c] and Jing Lu*[ade]

Received 9th February 2019
Accepted 13th May 2019

DOI: 10.1039/c9ta01509d

rsc.li/materials-a

Layered gallium sulphide (GaS) with hexagonal symmetry is a typical metal mono-chalcogenide and is mechanically stable under tension. In this work, we used first-principles density functional theory to study the performance of monolayer (ML) GaS as an anode material for Li, Na, K, Mg, and Al-ion batteries. The most stable binding sites for the metal atoms on ML GaS are all in the hollow sites, and the Fermi level of ML GaS moves upward into the conduction band after adsorption of Li, Na, K, and Al atoms, showing a semiconductor-to-metal transition of ML GaS, with the exception of Mg atoms. The binding energies of the metal atoms with ML GaS are all negative at all the studied densities, indicating a steady adsorbing process. The Li, Na, K, and Al ions prefer to move along the zigzag direction on ML GaS, with relatively low diffusion barrier heights of 0.110, 0.078, 0.037, and 0.034 eV, respectively. Such low diffusion barriers endow ML GaS with high rate capacity. The maximum theoretical specific capacities for Li, Na, K, and Al-ion batteries are 526.74, 32.92, 32.92, and 98.76 mA h g^{-1}, respectively. Noticeably, the theoretical specific capacity of ML GaS for Li-ion batteries (LIBs) is even higher than the theoretical one (372 mA h g^{-1}) of commercially used graphite. Besides, an appropriate average open circuit voltage of 0.53 V is generated for ML GaS based LIBs. Our study suggests that ML GaS is a suitable anode material for LIBs.

1 Introduction

The rapid progress of many electronic devices, such as portable electronic devices, electric vehicles and electricity grid systems, continuously increases the demand for advanced batteries with better performances.[1] Among the varieties of advanced batteries, rechargeable metal ion batteries (IBs), especially Li-ion batteries (LIBs), are the most widely used in both industrial and commercial fields. However, the limited capacities of current anode materials are typically a big hindrance to the deployment in the transportation sector. Two dimensional (2D) materials were recently found to be more favorable as electrode materials for IBs, due to their fully exposed flat surface, which contributes to ion diffusion and maximal metal atom accommodation sites, and thus can provide large rate and specific capacity for IBs.[2,3] 2D electrodes are demonstrated to have better performance than their bulk counterparts when used as electrode materials for LIBs. For instance, EunJoo *et al.* demonstrated that the performance of graphene nanosheets was superior to that of graphite when used as an anode in LIBs. They have a specific capacity of 540 mA h g^{-1} in graphene nanosheets in experiments,[4] which was higher than that of graphite (372 mA h g^{-1}) achieved through a first-principles study.[5] In addition, as the thickness of layered MoS_2 nanosheets decreases, the electrochemical performance is enhanced greatly,[6] and the diffusion barrier height also decreases from 0.47 eV (for bulk MoS_2) to 0.21 eV (for monolayer (ML) MoS_2).[7]

Up to now, many 2D electrodes for LIBs have been explored both theoretically and experimentally.[8–10] The graphite anode is commonly used commercially for LIBs because of its stability and low cost, but the low specific capacity cannot meet the growing requirements of technologies such as advanced electric vehicles. Graphitic carbon nitride (g-C_3N_4) has drawn growing attention due to its cost-effective availability, but the g-C_3N_4 anode shows a low initial discharge capacity (135 mA h g^{-1} in experiment).[11,12] MXenes (*e.g.*, Ti_3C_2, Ti_2C, and Mo_2C)[9,10,13,14] also exhibit a low specific capacity due to their metal-rich composition, which greatly reduces the adsorption ability of metal atoms.[15] The silicon anode has been intensively studied and has

[a]State Key Laboratory for Mesoscopic Physics and Department of Physics, Peking University, Beijing 100871, P. R. China. E-mail: jinglu@pku.edu.cn
[b]Academy for Advanced Interdisciplinary Studies, Peking University, Beijing 100871, P. R. China
[c]School of Advanced Materials, Peking University, Shenzhen Graduate School, Shenzhen 518055, P. R. China. E-mail: panfeng@pkusz.edu.cn; zhengjx@pkusz.edu.cn
[d]Collaborative Innovation Center of Quantum Matter, Beijing 100871, P. R. China
[e]Key Laboratory for the Physics and Chemistry of Nanodevices, Department of Electronics, Peking University, Beijing 100871, P. R. China

† Electronic supplementary information (ESI) available. See DOI: 10.1039/c9ta01509d

the known highest specific capacity (4200 mA h g^{-1}). However, it usually suffers from large volume expansion (300%) upon lithium insertion, leading to subsequent pulverization or mechanical fracture of silicon.[16–18] Black phosphorene is considered as a promising candidate anode material because its theoretical capacity can reach as high as 2596 mA h g^{-1} and ion diffusion barrier height can be as low as 0.08 eV,[19,20] but its poor stability leads to rapid degradation when exposed to air.[21,22] Some transition metal dichalcogenides (TMDs) have been proposed for use as anode materials, such as MoS_2,[7,23,24] VS_2,[25] ReS_2,[26] and WS_2.[27] They present moderately high specific capacities (400–900 mA h g^{-1}) but the diffusion barrier heights for Li ions are high (0.21–0.33 eV), which means that Li ions would have a low diffusion velocity during charging/discharging processes. Numerous other 2D materials also have low capacities as anode materials. For example, germanene,[28] IP_3 (ref. 3) and stanene[28] have specific capacities for LIBs of about 369, 258, and 226 mA h g^{-1}, respectively. The electrochemical performances can sometimes be improved through nanotube or nanowire arrays, carbon coating, *etc.*, but the complex fabrication process and high synthesis costs prevent their industrial applications.[22] In addition to LIBs, Na-ion batteries (NIBs),[3,15,29,30] K-ion batteries (KIBs),[31] Mg-ion batteries (MIBs),[32] and Al-ion batteries (AIBs)[9,33] have also been recently explored due to the abundance of these metal elements in the earth's crust as well as the similar electrochemical properties to Li atoms.[34,35] Nevertheless, continuing efforts have been made to the exploration of novel 2D materials that are suitable to be used as anodes for IBs with higher capacity.

2D metal mono-chalcogenide materials have attracted significant attention. Many of them have been fabricated in experiments[36,37] and demonstrate significantly different electronic characteristics from the TMDs. However, they are rarely explored as electrodes in IBs. ML gallium sulfide (GaS) with a hexagonal structure is a member of 2D metal mono-chalcogenides, and consists covalently bonded S–Ga–Ga–S atoms in each sheet (Fig. 1)[38,39] and has been fabricated through mechanical exfoliation on the substrate of SiO_2/Si using adhesive tape.[40–42] ML GaS is believed to be a suitable candidate for anode materials as it has the lowest molecular mass among these metal mono-chalcogenide materials, and the low molecular mass greatly contributes to the gravimetric specific capacity of an anode. Besides, ML GaS is expected to have very high diffusion velocity for metal atoms because of the special groove structure. The metal atoms would be trapped to move along the groove direction (one direction), which greatly shortens the moving distance of the metal atoms.[19] We expect that ML GaS would have high specific capacity when used as an anode material for rechargeable IBs.

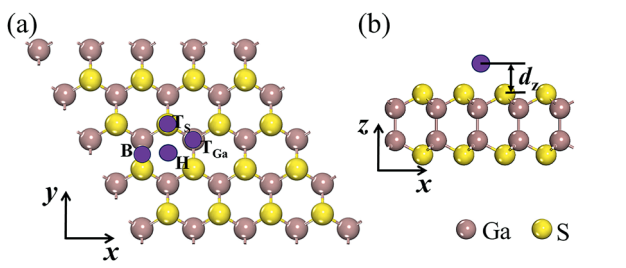

Fig. 1 Top (a) and side (b) views of the ML GaS structure. The purple dots indicate the different adsorbing sites.

2. Computational details

Calculations were carried out using density functional theory (DFT) in conjunction with the exchange correlation energy described by the generalized gradient approximation (GGA) in the scheme proposed by Perdew–Burke–Ernzerhof (PBE) as implemented in the Vienna *ab initio* simulation package (VASP).[43] Periodic boundary conditions are applied in all directions with a vacuum space of at least 15 Å in the *z* direction between adjacent GaS layers in order to avoid image–image interactions. Van der Waals interaction is taken into account using the semi-empirical correction of the DFT-D3 approach. Meanwhile, dipole correction is also used to remove the spurious interaction of the dipole moments induced by periodic images in the *z* direction. The projector-augmented wave (PAW) method with a cutoff energy of 400 eV is employed in this study. The structures of metal atom-ML GaS are firstly treated with the conjugate gradient algorithm to relax the ions and the lattice parameters for their energy minimization. For this step, a *k*-mesh density of 0.04 $Å^{-1}$ in the Monkhorst–Pack method[44] is sampled in the Brillouin zone with a convergence threshold of 10^{-5} eV for energy and 0.01 eV $Å^{-1}$ for force. After successful completion of the structure optimization, a single point calculation with a *k*-mesh density of 0.02 $Å^{-1}$ and an energy convergence threshold of 10^{-6} eV is performed to obtain the total energies and electronic properties of the systems such as the partial density of states (PDOS) and the charge density difference. This is followed by Bader charge analysis[45] and electron localization function (ELF) analysis in order to estimate the charge distribution situations. Finally, the charge capacity and open circuit voltage (OCV) are reported. The climbing image nudged elastic band (CI-NEB) method implemented in VASP transition state tools is used to determine the metal cationic minimum energy diffusion pathways and the corresponding energy barriers.

3 Results and discussion

3.1. Adsorption ability of the metal atoms on the surface of ML GaS

Knowing exactly the favorable adsorption sites is a fundamental requirement to evaluate the adsorption of the metal atoms on the surface of ML GaS. We simulate a 4 × 4 ML GaS supercell with one of the metal atoms located above to investigate the adsorption properties, and such a supercell is large enough to avoid the interaction between the metal atoms in different supercells. Four types of high symmetry adsorption sites are considered (Fig. 1(a)): the hollow site above the center of the hexagon (H site), the site on the top of a Ga atom (T_{Ga} site), the site on the top of a S atom (T_S site), and the site on a bond of Ga–S (B site). After full geometric optimization, all the studied

metal atoms initially on the T_S site move to the H site, and those initially on the B site move to the T_{Ga} site, but the metal atoms on the H site and the T_{Ga} site remain in their initial place and the corresponding geometrical structures are shown in Fig. 2 ((a–e) for the H site and (f–j) for the T_{Ga} site). The binding energy (E_b) can be defined as

$$E_b = \frac{E_{M_xGaS} - E_{GaS} - nE_M}{n}$$

where E_{M_xGaS}, E_{GaS}, and E_M are the total energy of ML GaS adsorbed by the metal atoms, pristine ML GaS, and a metal atom (M = Li, Na, K, Mg, and Al), respectively, and n is the number of metal atoms adsorbed on ML GaS. A solo metal atom is simulated by building a large supercell (10 × 10 × 10 Å) and putting one metal atom therein. According to the above definition, the more negative the binding energy for a metal atom adsorption on ML GaS, the more favorable the exothermic and spontaneous reaction between the metal atoms and ML GaS.

Spin-polarization correction is also used in our calculations, but it has a tiny effect on our results. For example, the total energy calculated with spin-polarization correction for pristine ML GaS and Li-doped ML GaS is the same as that calculated without the spin-polarization correction (−17.20 eV for a pristine ML GaS unit cell and −19.48 eV for Li-doped ML GaS with one Li atom adsorption on a ML GaS unit cell). The spin-polarization correction is not considered in our remaining calculations.

The E_b for Li, Na, K, Mg, and Al atoms adsorbing on the H site are −1.70, −1.27, −1.55, −0.38 and −1.32 eV per atom, respectively, and those on the T_{Ga} site are −1.58, −1.15, −1.49, −0.37, and −1.31 eV per atom, respectively. The absolute values of E_b on the H site are all larger than those on the T_{Ga} site, indicating that all five metal atoms are more likely to stay on the H site. Therefore, in the following discussion, we only focus our attention on the H site adsorption. The distance from the metal atoms at the H site to the ML GaS layer (d_Z) (Fig. 1(b)) in the sequence from small to large is 1.25 (Li), 1.86 (Na), 1.88 (Al), 2.29 (K), and 2.83 Å (Mg), respectively. The Mg atom has the largest distance from the surface of ML GaS and also the smallest binding energy with ML GaS. The absolute values of the E_b for Li, Na, K, and Al-atom adsorption on graphene (−1.10, −0.46, −0.80, and −1.04 eV per atom, respectively)[46] are smaller than those on ML GaS, indicating the stability of these metal atoms–ML GaS systems.

3.2. Electronic properties of the M/GaS configuration

The partial density of states (PDOS) for pristine ML GaS and the most stable metal atom adsorption configurations are depicted in Fig. 3(a–f). The PDOS structures show that the conduction band of ML GaS is mainly contributed by the p_x + p_y and s orbitals, and the valence band is mainly contributed by the p_z orbital. Generally, the overall PDOS structures of ML GaS are not significantly changed after the adsorption of the metal atoms, but just the Fermi level shifts up into the conduction bands, rendering a semiconductor-to-metal transition in ML GaS except for the adsorption of the Mg atom. The Fermi level of ML GaS also moves upward after adsorption of the Mg atom but does not shift into the conduction bands, making ML GaS not a conductor of electrons. This indicates that ML GaS is unsuitable for MIBs. The semiconductor-to-metal transition of ML GaS provides good electrical conductivity in the charge–discharge cycle. The PDOS of pristine Li, Na, K, and Al atoms (Fig. 3(b–d) and (f) inset) has an abundance of electron states around the Fermi level, but after adsorption on ML GaS, the electron states around the Fermi level decrease, and the electron states mainly contribute to the conduction bands. This indicates that the Li, Na, K, and Al atoms have been ionized after adsorption on ML GaS. The PDOS of the Mg atom has very small variation upon adsorption on ML GaS and both of them have an abundance of electron states around the Fermi level (Fig. 3(e) inset), indicating that the Mg atom is only slightly

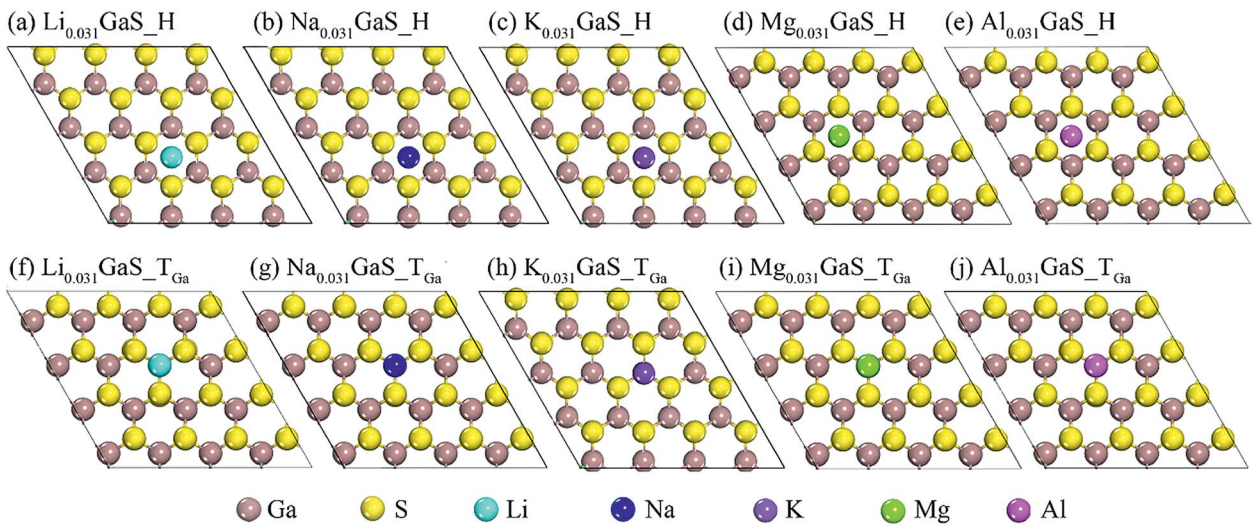

Fig. 2 Top view of the atomic structure of Li (a and f), Na (b and g), K (c and h), Mg (d and i) and Al (e and j) atoms adsorbing on the H site and T_{Ga} site of ML GaS.

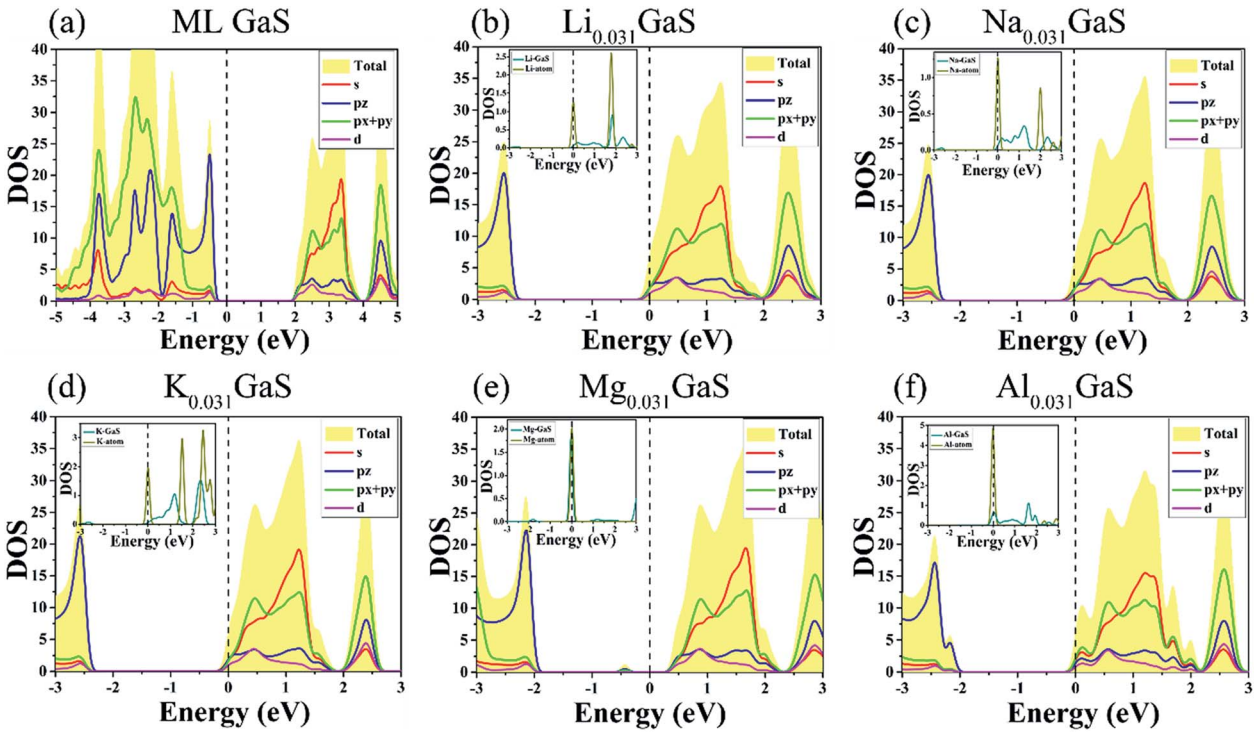

Fig. 3 Total density of states and projected density of states (PDOS) of pristine ML GaS (a) and ML GaS adsorbed by Li (b), Na (c), K (d), Mg (e), and Al (f) atoms. The insets are the PDOS of the adsorbed metal atoms and the DOS of the isolated metal atoms.

ionized on ML GaS. Such a performance reasonably explains the very small upshift of Fermi level of ML GaS after adsorption of the Mg atom.

The DFT-PBE method may give an underestimated bandgap for pristine ML GaS, but for the electron-doped ML GaS, the screening effect between electrons is increased and the interaction between the electrons is greatly reduced, and therefore the single particle approximation on which the DFT-PBE method is based is a good approximation to estimate the bandgap. For example, the calculated transport gaps with the DFT-PBE method for ML, bilayer, and trilayer black phosphorene (BP) are about 1.01, 0.81, and 0.69 eV, respectively.[47–49] The respective measured transport gaps, which reflect the bandgaps of a degenerately n-doped system, for ML, bilayer, and trilayer black phosphorene (BP) are 1.00, 0.71, and 0.61 eV, respectively.[50] By contrast, the HSE06 bandgaps for n-doped ML, bilayer, and trilayer BP are 1.52, 1.01, and 0.75 eV, respectively, according to the invariance of the bandgap with the doping in HSE06 calculations,[51] which are apparently larger than the experimental ones. For another example, the bandgap of the n-doped $MoSe_2$ calculated with DFT-PBE method (1.53 eV) is in accordance with that calculated with the most accurate GW method (1.59 eV) and the experimental result (1.58 eV).[52]

Our main purpose to calculate the PDOS of the structure is to investigate whether ML GaS can conduct electrons after adsorption of metal atoms. ML GaS, which is adsorbed with the metal atoms, is highly n-doped by electrons, and the DFT-PBE method is good enough to estimate the electronic properties of such n-doped systems.

During the charging process in an actual ion battery, the metal ions leave the cathode and move through the electrolyte into the anode. The electrons also move from the cathode but through the external circuits into the anode. The atoms still exist in the ionic state after getting to the anode. Our calculations based on VASP code can only simulate the static state, *i.e.*, the state where the metal ions have reached the anode. Bader charge analysis[53] indicates that Li, Na, K, Mg, and Al atoms act as the electron donors, and donate about $0.88e^-$, $0.84e^-$, $0.88e^-$, $0.21e^-$, and $0.75e^-$ per metal atom to the underlying ML GaS substrate, respectively. The Li, Na, K, and Al atoms exist in the ionic state after adsorption on ML GaS, which is in accordance with the PDOS analysis results and the practical situation, although the Al atoms are not fully ionized. The Mg atoms are only slightly ionized because of the low charge transfer, which is also in accordance with the PDOS analysis of the Mg-ML GaS system.

In order to get further insight into the interaction between the metal atoms and ML GaS substrate, the charge density difference ($\Delta\rho$) between the metal atoms and ML GaS is also calculated and is depicted in Fig. 4. $\Delta\rho$ is defined as $\Delta\rho = \rho_{M_xGaS} - \rho_{GaS} - \rho_M$, in which ρ_{M_xGaS}, ρ_{GaS}, and ρ_M represent the charge density values of ML GaS adsorbed with the metal atoms, pristine ML GaS, and the metal atoms, respectively. There is a net electron loss above the Li, Na, K, and Al atoms, and a net electron gain between metal atoms and the nearby S atoms, indicating the transfer of electrons from the metal atoms to ML GaS.[54] According to the above discussion and analysis, the adsorbed metal atoms donate their electrons to ML GaS and

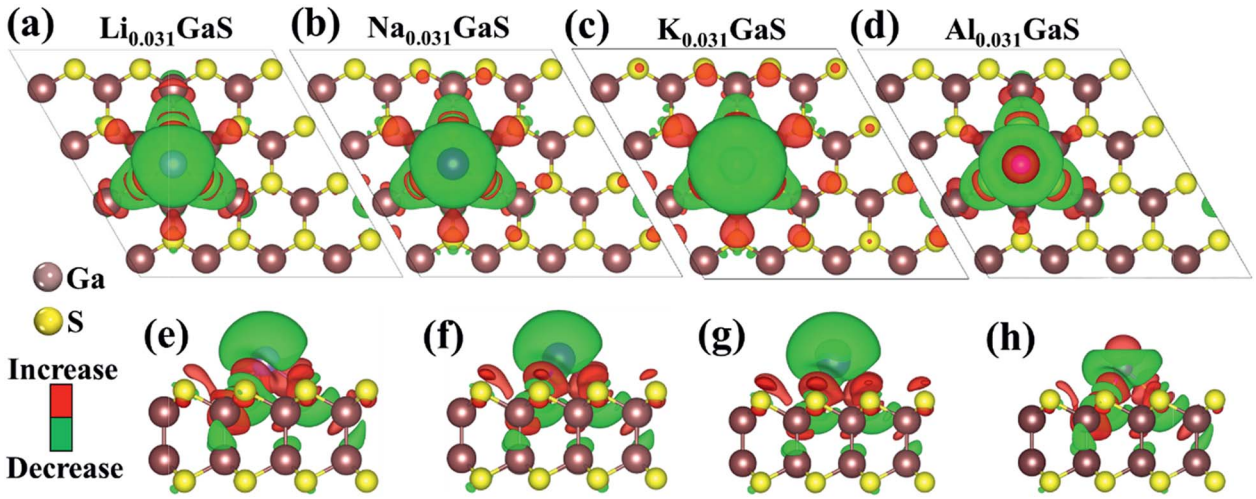

Fig. 4 Top (a–d) and side (e–h) views of charge density difference for ML GaS adsorbed by Li (a and e), Na (b and f), K (c and g), and Al (d and h) atoms.

exist in the ionic state. They can form a strong Coulomb interaction with ML GaS.

3.3. Diffusion of the metal ions on the surface of ML GaS

The migration path and barrier height of the metal ion diffusion on ML GaS are indispensable to evaluate their performance in batteries. The diffusion barrier height determines the charge–discharge rate of a rechargeable battery. As the metal atoms are ionized after adsorption on the surface of ML GaS, the entities that diffuse on the surface of ML GaS should be ions other than atoms. We examine the optimal diffusion paths and calculate the corresponding diffusion barriers by the CI-NEB method. We initially linearly inset the medial diffusion points both along the zigzag and armchair directions between two nearest neighboring H sites (the most favorite binding sites) on ML GaS. After optimization through the CI-NEB method, the inserted medial point gets to their saddle point along the zigzag ($H \rightarrow T_{Ga} \rightarrow H$) and the armchair directions ($H \rightarrow T_S \rightarrow B \rightarrow T_{Ga} \rightarrow H$) (Fig. 5(a)). Thus, the metal ions wouldn't choose to move linearly similar to metal ions moving on $NbSe_2$.[55] The diffusion energy profiles are shown in Fig. 5 ((b) for the zigzag and (c) for the armchair directions). The diffusion barrier heights along the zigzag direction are 0.110, 0.078, 0.037, and 0.034 eV for Li, Na, K, and Al ions, respectively, and the corresponding pathway lengths are all about 4.25 Å (Fig. 5(b)). The T_{Ga} site is a sunken site along the energy profiles and is only energetically higher than the H site by about 0.043, 0.043, 0.018, and 0.022 eV for Li, Na, K, and Al ions, respectively. S_1 and S_2 are the saddle points along the energy profile. The diffusion barrier heights along the armchair direction for Li, Na, K, and Al ions are 0.502, 0.338, 0.249, and 0.198 eV, respectively, and the corresponding pathway lengths are all about 6.53 Å (Fig. 5(c)). The saddle point along the energy profile in the armchair direction is at the T_S site. The T_{Ga} site is a sunken site and is marginally energetically higher than the H site by about 0.029, 0.039, 0.005, and 0.005 eV for Li, Na, K and Al ions, respectively. The diffusion barrier heights along the zigzag direction are about one order of magnitude smaller than those along the armchair direction, and the corresponding pathway lengths are also shorter than those along the armchair direction. Obviously, the metal ions prefer to migrate along the zigzag direction rather than the armchair direction on ML GaS because of the much lower diffusion barrier heights and the pathway lengths.

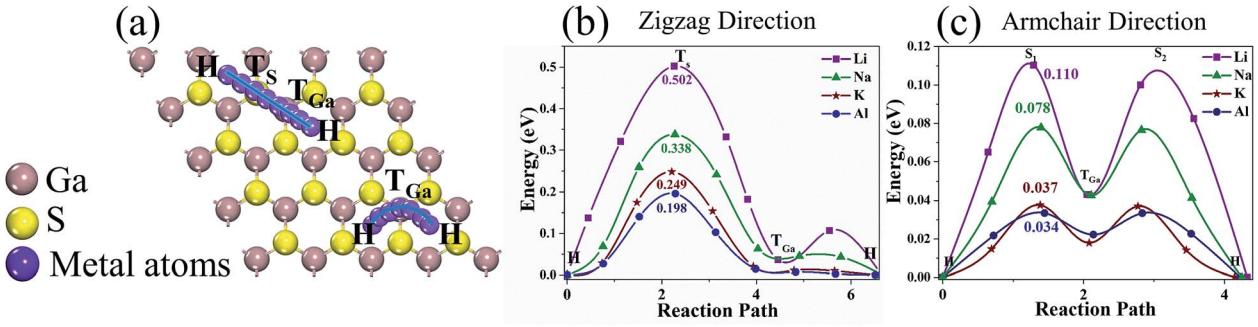

Fig. 5 Diffusion energy barrier (a) for Li, Na, K, and Al ions that diffuse on the surface of ML GaS along the zigzag (b) and armchair (c) direction pathways.

We can conclude that the ion diffusion barrier heights follow the order of $Li^+ > Na^+ > K^+ > Al^{3+}$. The molecular diffusion constant (D) of metal-ions, which is temperature-dependent, can be estimated using the Arrhenius equation,[56]

$$D \sim \exp\left(\frac{-E_a}{k_B T}\right)$$

where E_a and k_B are the diffusion barrier height and Boltzmann's constant, respectively, and T is the environmental temperature. The diffusion velocities of Na, K, and Al ions are about three times, 17 times, and 19 times higher than that of Li ions on ML GaS, respectively.

Li ions have the highest diffusion barrier height among the four metal ions and thus very rarely migrate to the ML GaS surface. But the diffusion barrier height of Li ions on ML GaS is still much smaller than that on graphene (0.33 eV).[57] The velocity of Li ion diffusion on ML GaS is about 10^3 times as fast as that on graphene. Besides, the diffusion barrier height is also smaller than those of many other anode materials such as ML MoS_2 (0.21 eV),[7] ML VS_2 (0.22 eV),[25] and silicene (0.23 eV).[58] Therefore, Li ions have a wonderful high-rate capacity performance on ML GaS. Other studied metal-ions (Na, K, and Al), which have smaller diffusion barrier heights, would have better high-rate capacity performance on ML GaS.

The diffusion of Na ions on ML GaS has the second highest diffusion barrier height, and the diffusion barrier height is smaller than that of Na ions on ML TiC_3 (0.18 eV).[15] The velocity of Na ion migration on ML GaS is about 50 times larger than on ML TiC_3. The diffusion barrier height for K ions on graphite at low K density is about 0.16 eV,[59] which makes the velocity about 10^2 times slower than that on ML GaS. Therefore, high-rate capacity performance can be expected for ML GaS used as an anode material for LIBs, NIBs, KIBs, and AIBs.

3.4. Li storage capacity and open circuit voltage

The specific capacity of anode materials is proportional to the number of maximum adsorbed metal atoms. We investigate the concentration-dependent adsorption behavior of the metal atoms on ML GaS. Through putting one metal atom at the most stable binding site (the H site) in a 4×4, 3×3, 2×2, and 1×1 supercell in sequence, we get the configuration of M_xGaS (M = Li, Na, K, Al) (Fig. S1†) with the metal-ion density ($x = 0.031$, 0.056, 0.125, 0.5) from low to high. In such a sequence, the metal atoms are distributed uniformly on the surface of ML GaS, and thus they could stay with inter-atomic distance as large as possible to avoid the Coulomb repulsive force. A higher metal concentration is only useable for Li atoms, and the configurations of Li_xGaS ($x = 1$, 1.5, 2, 2.5) are obtained through adding Li atoms one by one at the most stable binding sites on the 1×1 supercell of ML GaS (Fig. S2†). The adsorption order follows the minimum energy pathway.

With the increasing density of metal atom adsorption on ML GaS, the distance between the metal atoms decreases, the interaction between the metal atoms increases, and the metallic bonds have larger possibility to be formed among the metal atoms. The metallic bonds with the metal atoms are unexpected because very dangerous dendritic growth may appear in such a system. ELF is an effective method for revealing whether metallic bonds are formed or not between metal atoms (Fig. S3–6†). If the space between the metal atoms is full of free electron gas states (ELF ~ 0.5), metallic bonds are formed between these metal atoms. However, if the regions are separated by the trajectories of minimal function values of ELF,[60] metallic bonds cannot be formed between the metal atoms.

The maximum theoretical capacity (C) can be obtained from

$$C = \frac{1}{M_{GaS}} \times z \times x_{max} \times F$$

where x_{max} represents the highest concentration of Li ions; z is the valence number of the metal atoms ($z = 1$ for Li, Na, and K, and $z = 3$ for Al atoms); F is the Faraday constant; and M_{GaS} is the atomic molar weight of bulk or ML GaS.

There are always regions with ELF ~ 0 between Li atoms (Fig. S3(b)†), and Bader charge analysis indicates that Li atoms donate about $0.94e^-$ per Li atom to ML GaS even at very high Li density ($Li_{2.5}GaS$), indicating metallic bonds are not formed between each Li atom. But at $x = 2.5$, after releasing the Li atoms, ML GaS cannot return to its initial structure. At $x = 2$, ML GaS returns to its initial structure after releasing the Li atoms. Thus, the highest Li density for ML GaS is Li_2GaS (Fig. 7(a)), and such a density corresponds to a theoretical capacity of 526.74 mA h g^{-1}. The theoretical capacity is larger than those of many other theoretically studied anode materials such as Ti_3C_2 (320 mA h g^{-1}),[13] Ti_2N (484 mA h g^{-1}), and Ti_2NO_2 (378 mA h g^{-1}), and even larger than that of the commercially used graphene (326 mA h g^{-1}). Thus, ML GaS is good enough to satisfy the requirement of high capacity. At the highest Li-ion density, the binding energy for Li ion adsorption on ML GaS is smaller than the cohesive energy of the Li-metal, demonstrating that Li atoms can be stably adsorbed and the dendritic growth can be avoided.[61]

The Na and Al atoms form metallic bonds with each other at $x = 0.5$ as there is an electron gathering layer with ELF > 0.5 upon Na and Al atoms (Fig. S4(b) and S5(b)†). But there are trajectories of minimal function values between metal atoms at $Na_{0.125}GaS$ (Fig. S4(a)†) and $Al_{0.125}GaS$ (Fig. S5(a)†). Bader charge analysis indicates that Na and Al atoms donate about $0.30e^-$ per Na atom and $0.28e^-$ per Al atom, respectively, at $x = 0.5$, and the low charge transfer supports the metallic bond formation between the metal atoms as distinguished in the ELF results. Besides, the geometric structure of ML GaS has no change even at $Na_{0.125}GaS$ and $Al_{0.125}GaS$, which indicates that ML GaS can certainly return to its initial structure after releasing of the metal atoms. Thus, the highest Na and Al density adsorptions on ML GaS are $Na_{0.125}GaS$, and $Al_{0.125}GaS$ and the corresponding theoretical capacities are 32.92 mA h g^{-1} and 98.76 mA h g^{-1}, respectively. Such theoretical capacities for Na and Al are lower than other theoretically studied 2D anode materials. For example, the theoretical capacity for Na ions on Ti_2N is 484 mA h g^{-1}, on Ti_2NO_2 is 378 mA h g^{-1}, and on Ti_2NF_2 is 181 mA h g^{-1}.[62] The theoretical capacity for Al ions on graphite is about 100 mA h g^{-1},[33] and that is 1134 mA h g^{-1} for

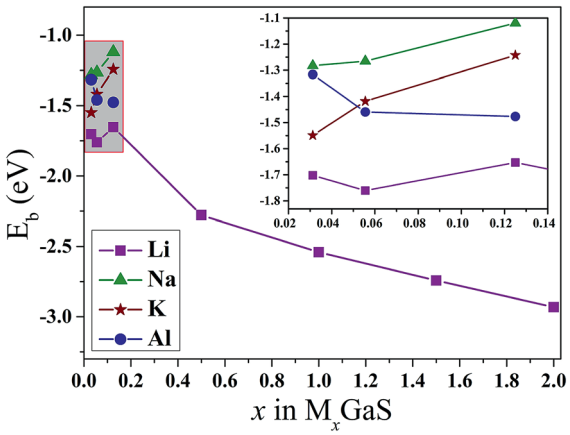

Fig. 6 Binding energy as a function of x in ML M_xGaS.

Al ions on Ti_2NO_2.[62] So, pristine ML GaS may not be suitable as an anode for NIBs and AIBs.

As for K atoms, there are minimal function value regions with ELF ~ 0.3 between K atoms at $K_{0.5}GaS$ (Fig. S6(b)†) but full of regions of ELF ~ 0.5 at K_1GaS (Fig. S6(c)†). K atoms still do not form metallic bonds at $x = 0.5$ as Na and Al atoms do possibly because of the smaller electronegativity of K atoms. Bader charge analysis indicates that K atoms donate about $0.32e^-$ per K atom, and the value is a little larger than that for Na and Al atoms at $x = 0.5$. But the number of electrons transferred from K atoms to ML GaS at $x = 0.5$ is still low and K atoms are only slightly ionized. K atoms donate about $0.65e^-$ per K atom at $x = 0.125$ and exist in the ionic state at such densities. Besides, the ELF map (Fig. S6(a)†) shows that there is minimum function value between each K atom and no metallic bonds are formed at $x = 0.125$. The geometry structure of $K_{0.125}GaS$ is also almost unchanged and ML GaS can return to its initial geometric structure after releasing the K atoms. Thus, the highest K density for ML GaS is $K_{0.125}GaS$, the same as Na and Al atoms, and the theoretical capacity is also 32.92 mA h g^{-1}. So, pristine ML GaS is also not suitable to be used as an anode for KIBs.

According to our calculations, there are two parameters, which are the diameter and the electronegativity of the metal atoms that affect the adsorption properties of the metal atoms on ML GaS. The metal atoms have the diameter (d) order of $d_{Li} < d_{Al} < d_{Mg} < d_{Na} < d_K$ and the electronegativity (NE) order of $NE_K < NE_{Na} < NE_{Li} < NE_{Mg} < NE_{Al}$. The small diameter would help the metal atoms like Li atoms get into ML GaS and thus have strong interaction with ML GaS, and metallic bonds are rarely formed between the metal atoms. The small electronegativity means that the metal atoms like K atoms are more likely to lose their electrons and also are rarely likely to form metallic bonds with themselves. Na atoms have a relatively large diameter but small electronegativity, and Al atoms have relatively large electronegativity but a small diameter, and they can make ML GaS undergo a semiconductor-to-metal transition, but they would form metallic bonds with themselves on ML GaS at low density. Mg atoms have the medium diameter and relatively large electronegativity and cannot donate its electrons to ML GaS even at low density.

The binding energies for all the metal atom adsorption on ML GaS at all the studied densities are all negative, indicating that the adsorption process is spontaneous and the good stability of the metal atoms–ML GaS system. The binding energy for Li atoms decreases as the density of the metal atoms increases except at $x = 0.125$ (Fig. 6), where the binding energy increases a little. The decreasing binding energies with the increasing metal atom density is tentatively attributed to the small atomic diameter of Li ions, and thus the metal atoms can move into ML GaS (Fig. S3†) other than just being adsorbed on the surface. The binding energy for Al atoms also decreases as Al

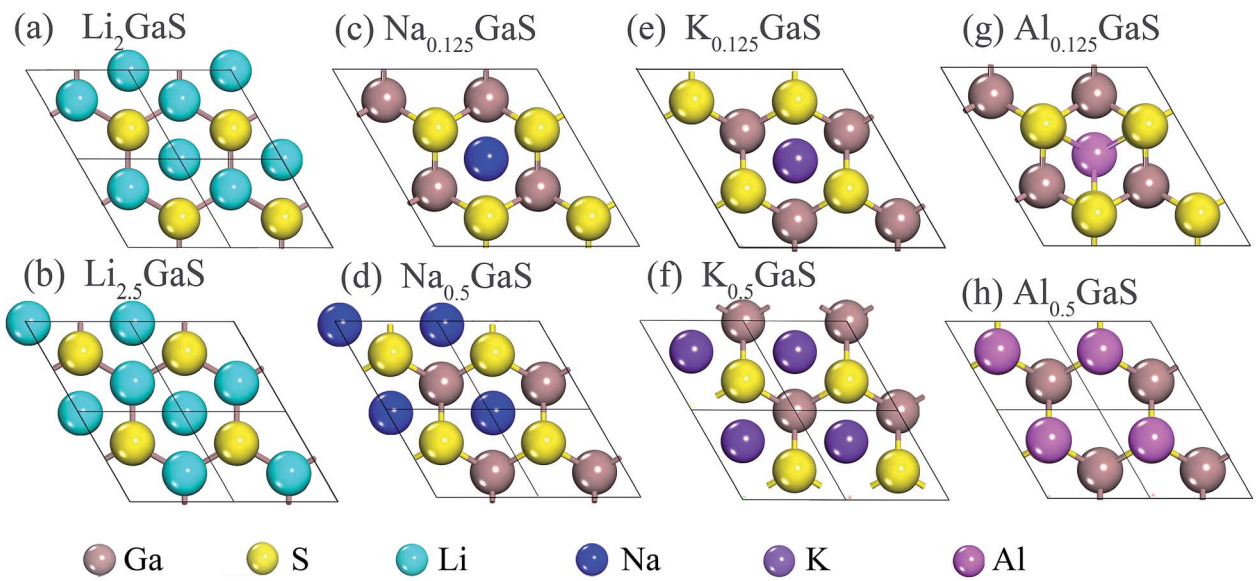

Fig. 7 Geometry structure of ML Li_2GaS (a), $Li_{2.5}GaS$ (b), $Na_{0.125}GaS$ (c), $Na_{0.5}GaS$ (d), $K_{0.125}GaS$ (e), $K_{0.5}GaS$ (f), $Al_{0.125}GaS$ (g) and $Al_{0.5}GaS$ (h).

atom density increases because the diameter of Al is also small. But the binding energy for Na and K atoms increases as the density increases because of their large atomic diameter. The decreasing binding energy indicates that Li atoms are easier to be absorbed at higher density, which is beneficial for the application of ML GaS used as an anode material for Li and Al-ion batteries.

Furthermore, the OCV is a crucial parameter that reflects the electrode performance, which can be estimated by calculating the average voltage over a range of metal atom composition domains in theory.[63–65] As ML GaS is only suitable to be used in LIBs, we only calculate the OCV for Li_xGaS in our study. The average voltage of Li_xGaS in the range of $x_1 \leq x \leq x_2$ can be defined as

$$V \approx \frac{E_{Li_{x1}GaS} - E_{Li_{x2}GaS} + (x_2 - x_1)E_{metal}}{(x_2 - x_1)e}$$

where $E_{Li_{x1}GaS}$, $E_{Li_{x2}GaS}$, and E_{metal} are the energy of $Li_{x1}GaS$, $Li_{x2}GaS$, and metallic Li, respectively. We get the average voltage through our calculation for LIBs and it is about 0.53 V. The low average OCV of anode materials would contribute to a high energy density. But a too low OCV for the anode would result in metal plating. A suitable voltage for an anode material is in the range of 0.2–1.0 V.[10] The OCV for ML GaS based LIBs is just in this range. Thus, ML GaS can be a suitable anode material for LIBs.

4 Conclusion

In summary, we used first-principles density functional theory calculations to analyze Li, Na, K, Mg, and Al atom adsorption and diffusion properties on ML GaS. Our study indicates that ML GaS may not be suitable to be used in NIBs, KIBs, MIBs, and AIBs, but the performance of the ML GaS anode is superior in LIBs. Both high rate capacity with ion velocity 10^3 times as fast as that on graphene and high theoretical capacity (526.74 mA h g^{-1}, higher than those of many other layered anode materials) are obtained in LIBs. Besides, the average OCV of ML GaS for LIBs also falls into a suitable range (0.2–1.0 V), over which lithium plating can be avoided and high energy density can be guaranteed. What's more, the adsorption of Li-atoms makes the ML GaS transition into a metal state such that the ML GaS anode can conduct electrons perfectly. Finally, the Li atom is fully ionized on ML GaS and guarantees its ability of charge transfer. Thus, this work opens up the possibility of developing improved intercalation ML GaS electrodes for LIBs.

Conflicts of interest

There are no conflicts to declare.

Acknowledgements

This work was supported by the Ministry of Science and Technology of China (No. 2016YFB0700600 (National Materials Genome Project) and 2017YFA206303) and the National Natural Science Foundation of China (No. 11674005 and 11664026).

References

1 J. M. Tarascon and M. Armand, *Nature*, 2001, **414**, 359–367.
2 J. Liu and X.-W. Liu, *Adv. Mater.*, 2012, **24**, 4097–4111.
3 J. Liu, C.-S. Liu, X.-J. Ye and X.-H. Yan, *J. Mater. Chem. A*, 2018, **6**, 3634–3641.
4 E. Yoo, J. Kim, E. Hosono, H. S. Zhou, T. Kudo and I. Honma, *Nano Lett.*, 2008, **8**, 2277–2282.
5 K. Persson, Y. Hinuma, Y. S. Meng, A. Van Der Ven and G. Ceder, *Phys. Rev. B: Condens. Matter Mater. Phys.*, 2010, **82**, 125416.
6 H. Hwang, H. Kim and J. Cho, *Nano Lett.*, 2011, **11**, 4826–4830.
7 Y. Li, D. Wu, Z. Zhou, C. R. Cabrera and Z. Chen, *J. Phys. Chem. Lett.*, 2012, **3**, 2221–2227.
8 Z. Chen-Xi and L. Hong, *Energy Environ. Sci.*, 2011, **4**, 2614–2624.
9 M. R. Lukatskaya, O. Mashtalir, C. E. Ren, Y. Dall'Agnese, P. Rozier, P. L. Taberna, M. Naguib, P. Simon, M. W. Barsoum and Y. Gogotsi, *Science*, 2013, **341**, 1502–1505.
10 C. Eames and M. S. Islam, *J. Am. Chem. Soc.*, 2014, **136**, 16270–16276.
11 J. Chen, Z. Mao, L. Zhang, D. Wang, R. Xu, L. Bie and B. D. Fahlman, *ACS Nano*, 2017, **11**, 12650–12657.
12 X. H. Yang, H. J. Wang, X. F. Lu, D. L. Cui and S. Y. Zhang, *Acta Chim. Sin.*, 2009, **67**, 1166–1170.
13 Q. Tang, Z. Zhou and P. Shen, *J. Am. Chem. Soc.*, 2012, **134**, 16909–16916.
14 M. Naguib, J. Halim, J. Lu, K. M. Cook, L. Hultman, Y. Gogotsi and M. W. Barsoum, *J. Am. Chem. Soc.*, 2013, **135**, 15966–15969.
15 T. Yu, Z. Zhao, L. Liu, S. Zhang, H. Xu and G. Yang, *J. Am. Chem. Soc.*, 2018, **140**, 5962–5968.
16 B. A. Boukamp, G. C. Lesh and R. A. Huggins, *J. Electrochem. Soc.*, 1981, **128**, 725–729.
17 Q. Zhang, W. Zhang, W. Wan, Y. Cui and E. Wang, *Nano Lett.*, 2010, **10**, 3243–3249.
18 R. N. Seefurth and R. A. Sharma, *J. Electrochem. Soc.*, 1977, 974–977.
19 W. Li, Y. Yang, G. Zhang and Y.-W. Zhang, *Nano Lett.*, 2015, **15**, 1691–1697.
20 J. Sun, G. Zheng, H.-W. Lee, N. Liu, H. Wang, H. Yao, W. Yang and Y. Cui, *Nano Lett.*, 2014, **14**, 4573–4580.
21 J. H. Yang, Y. Zhang, W. J. Yin, X. G. Gong, B. I. Yakobson and S. H. Wei, *Nano Lett.*, 2016, **16**, 1110–1117.
22 J. Liu, S. Wang and Q. Sun, *Proc. Natl. Acad. Sci. U. S. A.*, 2017, **114**, 651–656.
23 Y. Lu, X. Yao, J. Yin, G. Peng, P. Cui and X. Xu, *RSC Adv.*, 2015, **5**, 7938–7943.
24 G. Du, Z. Guo, S. Wang, R. Zeng, Z. Chen and H. Liu, *Chem. Commun.*, 2010, **46**, 1106–1108.
25 Y. Jing, Z. Zhou, C. R. Cabrera and Z. Chen, *J. Phys. Chem. C*, 2013, **117**, 25409–25413.
26 S. Mukherjee, A. Banwait, S. Grixti, N. Koratkar and C. V. Singh, *ACS Appl. Mater. Interfaces*, 2018, **10**, 5373–5384.

27 R. Bhandavat, L. David and G. Singh, *J. Phys. Chem. Lett.*, 2012, **3**, 1523–1530.
28 B. Mortazavi, A. Dianat, G. Cuniberti and T. Rabczuk, *Electrochim. Acta*, 2016, **213**, 865–870.
29 L. E. Marbella, M. L. Evans, M. F. Groh, J. Nelson, K. J. Griffith, A. J. Morris and C. P. Grey, *J. Am. Chem. Soc.*, 2018, **140**, 7994–8004.
30 Y. Wen, K. He, Y. Zhu, F. Han, Y. Xu, I. Matsuda, Y. Ishii, J. Cumings and C. Wang, *Nat. Commun.*, 2014, **5**, 4033.
31 Z. Jian, W. Luo and X. Ji, *J. Am. Chem. Soc.*, 2015, **137**, 11566–11569.
32 B. Mortazavi, O. Rahaman, S. Ahzi and T. Rabczuk, *Appl. Mater. Today*, 2017, **8**, 60–67.
33 C. J. Pan, C. Yuan, G. Zhu, Q. Zhang, C. J. Huang, M. C. Lin, M. Angell, B. J. Hwang, P. Kaghazchi and H. Dai, *Proc. Natl. Acad. Sci. U. S. A.*, 2018, **115**, 5670–5675.
34 S. Chu, Y. Cui and N. Liu, *Nat. Mater.*, 2017, **16**, 16–22.
35 H. Kim, J. C. Kim, M. Bianchini, D. H. Seo, J. Rodriguez-Garcia and G. Ceder, *Adv. Energy Mater.*, 2018, **8**, 19.
36 J. R. Brent, D. J. Lewis, T. Lorenz, E. A. Lewis, N. Savjani, S. J. Haigh, G. Seifert, B. Derby and P. O'Brien, *J. Am. Chem. Soc.*, 2015, **137**, 12689–12696.
37 Y. J. Cho, H. S. Im, Y. Myung, C. H. Kim, H. S. Kim, S. H. Back, Y. R. Lim, C. S. Jung, D. M. Jang, J. Park, E. H. Cha, S. H. Choo, M. S. Song and W. I. Cho, *Chem. Commun.*, 2013, **49**, 4661–4663.
38 B. Wen, R. Melnik, S. Yao and T. J. Li, *Mater. Sci. Semicond. Process.*, 2010, **13**, 295–297.
39 E. Machado-Charry, E. Canadell and A. Segura, *Phys. Rev. B: Condens. Matter Mater. Phys.*, 2007, **75**, 7.
40 D. J. Late, B. Liu, H. S. S. R. Matte, C. N. R. Rao and V. P. Dravid, *Adv. Funct. Mater.*, 2012, **22**, 1894–1905.
41 P. Hu, L. Wang, M. Yoon, J. Zhang, W. Feng, X. Wang, Z. Wen, J. C. Idrobo, Y. Miyamoto, D. B. Geohegan and K. Xiao, *Nano Lett.*, 2013, **13**, 1649–1654.
42 D. J. Late, B. Liu, J. Luo, A. Yan, H. S. Matte, M. Grayson, C. N. Rao and V. P. Dravid, *Adv. Mater.*, 2012, **24**, 3549–3554.
43 J. P. Perdew, K. Burke and M. Ernzerhof, *Phys. Rev. Lett.*, 1996, **77**, 3865–3868.
44 G. Kresse and D. Joubert, *Phys. Rev. B: Condens. Matter Mater. Phys.*, 1999, **59**, 1758–1775.
45 R. F. W. Bader, *Chem. Rev.*, 1991, **91**, 893–928.
46 K. T. Chan, J. B. Neaton and M. L. Cohen, *Phys. Rev. B: Condens. Matter Mater. Phys.*, 2008, **77**, 235430.
47 Y. Pan, Y. Wang, M. Ye, R. Quhe, H. Zhong, Z. Song, X. Peng, D. Yu, J. Yang, J. Shi and J. Lu, *Chem. Mater.*, 2016, **28**, 2100–2109.
48 Y. Pan, Y. Dan, Y. Wang, M. Ye, H. Zhang, R. Quhe, X. Zhang, J. Li, W. Guo, L. Yang and J. Lu, *ACS Appl. Mater. Interfaces*, 2017, **9**, 12694–12705.
49 X. Zhang, Y. Pan, M. Ye, R. Quhe, Y. Wang, Y. Guo, H. Zhang, Y. Dan, Z. Song, J. Li, J. Yang, W. Guo and J. Lu, *Nano Res.*, 2018, **11**, 707–721.
50 S. Das, W. Zhang, M. Demarteau, A. Hoffmann, M. Dubey and A. Roelofs, *Nano Lett.*, 2014, **14**, 5733–5739.
51 Y. Cai, G. Zhang and Y. W. Zhang, *Sci. Rep.*, 2014, **4**, 6677.
52 Y. Liang and L. Yang, *Phys. Rev. Lett.*, 2015, **114**, 063001.
53 W. Tang, E. Sanville and G. Henkelman, *J. Phys.: Condens. Matter*, 2009, **21**, 084204.
54 X. Lv, W. Wei, Q. Sun, L. Yu, B. Huang and Y. Dai, *ChemPhysChem*, 2017, **18**, 1627–1634.
55 X. Lv, W. Wei, Q. Sun, B. Huang and Y. Dai, *J. Phys. D: Appl. Phys.*, 2017, **50**, 235501.
56 W. Li and Y. Mu, *Nanoscale*, 2012, **4**, 1154–1159.
57 C. Uthaisar and V. Barone, *Nano Lett.*, 2010, **10**, 2838–2842.
58 G. A. Tritsaris, E. Kaxiras, S. Meng and E. Wang, *Nano Lett.*, 2013, **13**, 2258–2263.
59 Z. Xu, X. Lv, J. Chen, L. Jiang, Y. Lai and J. Li, *Carbon*, 2016, **107**, 885–894.
60 A. Savin, R. Nesper, S. Wengert and T. F. Fassler, *Angew. Chem., Int. Ed.*, 1997, **36**, 1809–1832.
61 X. Lv, W. Wei, B. Huang and Y. Dai, *J. Mater. Chem. A*, 2019, **7**, 2165–2171.
62 D. Wang, Y. Gao, Y. Liu, D. Jin, Y. Gogotsi, X. Meng, F. Du, G. Chen and Y. Wei, *J. Phys. Chem. C*, 2017, **121**, 13025–13034.
63 M. K. Aydinol, A. F. Kohan, G. Ceder, K. Cho and J. Joannopoulos, *Phys. Rev. B: Condens. Matter Mater. Phys.*, 1997, **56**, 1354–1365.
64 F. Zhou, M. Cococcioni, C. A. Marianetti, D. Morgan and G. Ceder, *Phys. Rev. B: Condens. Matter Mater. Phys.*, 2004, **70**, 235121.
65 R. E. Doe, K. A. Persson, Y. S. Meng and G. Ceder, *Chem. Mater.*, 2008, **20**, 5274–5283.

